Preparation and characterization of Nextel™ 720/ alumina ceramic composites via the prepreg process

Hao Li
SCUT: South China University of Technology
Bo-xing Zhang
SCUT: South China University of Technology
Ying Guo
ICCAS: Institute of Chemistry Chinese Academy of Sciences
Weijian Han
ICCAS: Institute of Chemistry Chinese Academy of Sciences
Tong Zhao
ICCAS: Institute of Chemistry Chinese Academy of Sciences
Wenfeng Qiu (wfqiu@scut.edu.cn)
South China University of Technology https://orcid.org/0000-0002-4935-3267

Research Article

Keywords: ceramic matrix composite, alumina, prepreg, aqueous slurry, preceramic polymer

Posted Date: September 15th, 2021

DOI: https://doi.org/10.21203/rs.3.rs-898486/v1

Abstract

In this work, the continuous Nextel™ 720 fiber reinforced alumina ceramic matrix composites (CMCs) were prepared by the prepreg process. The alumina matrix derived from aqueous slurry, which consisted of organic glue, alumina sol, nanometer alumina powder and micrometer alumina powder. This combination endowed the ceramic matrix composite with the prepreg processing capability, making the low-cost fabrication of complex shape components possible. The ratio of different alumina sources in aqueous slurry was optimized to offer good sintering activity, high thermal resistance, and excellent mechanical properties simultaneously. Furthermore, the preceramic polymer of mullite was used to strengthen the ceramic matrix through multiple impregnation process. The final CMC sample achieved a high flexural strength of 255 MPa and a good high-temperature stability. The maximum flexural strength of the CMC sample still remained 85% after heat-treatment at 1100 ℃ for 24 h.

1. Introduction

In recent years, oxide-oxide ceramic matrix composites (CMCs) have attracted ever-increasing attentions in high-temperature aerospace areas due to their low density and the capability of maintaining excellent mechanical strength and fracture toughness up to 1100 ℃ in air [1–4]. Although, compared to conventional non-oxide CMC, such as SiC-based materials, oxide-oxide CMC have inferior mechanical performance, their inherent oxidation resistance gives more advantage on the long-term applications in the oxidative atmosphere [1].

Generally speaking, three aspects contribute to mechanical performance of CMC. The first one is reinforcement fibers, which play a crucial role in CMC with respect to reinforcement and flaw tolerance. For oxide-oxide CMC, common fiber species used in the research and industrial areas are continuous Nextel™ 610 and Nextel™ 720 fibers [2, 4–13]. Nextel™ 610 is a high-purity alumina fiber (> 99% Al_2O_3) [14]. Nextel™ 720 is an alumina-mullite fiber (85 wt% Al_2O_3 and 15 wt% SiO_2) with an alumina-mullite volume fraction ratio of 57:43 [15]. Their fiber tow contains 400 filaments with an average filament diameter of 12 μm. Nextel™ 610 has higher tensile strength (3.2 GPa) than Nextel™ 720 (2.1 GPa) at low and moderately high temperatures (up to approximately 1000 ℃) [16], but the latter possesses better creep resistance up to 1200 ℃ [9, 17]. Above 1200 ℃, both of Nextel™ 610 and Nextel™ 720 fibers are subjected to severe degradation of mechanical performance due to the rapid growth of crystalline grains.

The second one is ceramic matrix, which is commonly comprised of alumina, alumina-silica, or alumina-mullite [9], because that they can be partially sintered below 1200 ℃ and have excellent mechanical performance. However, it is not easy to uniformly fill these components into the ceramic fibric and make them stack closely due to the impediment of ceramic fibers. Also, these components are difficult to sinter and achieve good mechanical strength without the aid of pressure below 1200 ℃. Many researches have been done to solve these problems. Wang and Cheng et al. used diphasic Al_2O_3-SiO_2 sols as the precursor of aluminosilicate ceramic matrix, which had a good processing ability and a high sintering activity [18, 19]. However, the mechanical performance and high-temperature stability need to be further improved.

Jiang and Liu et al. used α-Al_2O_3 with a grain size of 200 nm as the matrix and Nextel™ 610 as the reinforcement fiber to fabricate CMC, whose flexural strength kept stable at 25-1050 ℃, while dramatically decreased at 1100–1200 ℃ [5]. Except for the growth of crystallites in fibers, we think that the shrinkage from the matrix may also be responsible for this result, since nanometer alumina powders had good sintering ability and could be steadily sintered above 1000 ℃. To resolve the contradiction between sintering activity and high-temperature stability, Levi and Evan et al. proposed an interesting route, in which large (~ 1 μm) mullite particles and small alumina particles (~ 200 nm) were used together. Large particles were packed between and within tows to form a touching, non-shrinking network, and small particles fitted within the void spaces of this network to form bridges between the larger mullite particles, as well as between the mullite particles and the fibers [17]. However, it was essential to use vacuum infiltration technique to fill the fiber preform with these particles. For large or thick CMC materials, defect might occur easily. Another attractive route for the matrix preparation was reaction-bonding aluminum oxide (RBAO) [20–22], in which metallic aluminum particles was added. The metallic aluminum particles will be oxidized and expanded during heat treatment in air to form alumina, obviating the shrinkage of the matrix in the presence of a rigid fiber network. However, special care should be taken to avoid the moisture during storage and processing, because fine metallic aluminum particles were highly active toward water.

In addition to the fiber and matrix, the interface between them also plays a vital role on the mechanical performance of CMC. Fugitive carbon coating [19], oxide rare-earth orthophosphates coating ($REPO_4$) [23–25], and porous matrix [26] are common strategies to overcome brittle fracture of CMC. In this study, in order to simplify the material system, no coating was engineered between fibers and matrix, and a porous matrix was designed to provide weak interface that was responsible to toughen CMC materials through debonding, crack deflection, and pulling out mechanism. We aim to develop an aqueous ceramic slurry, which could be used to prepare the matrix of high-temperature CMC by the prepreg process, and adapt to the fabrication of complex shape CMC components. Microstructure evolution and functions of different alumina components in aqueous slurry will be clarified. The preceramic polymer will be used to strengthen CMC, and its influence on mechanical performance of CMC will be systematically investigated. This study will shed light on the design and realization of the matrix of CMC materials.

2. Experimental

2.1 Materials

Reinforcement fibers used in this work were Nextel 720™ woven in an eight-harness satin weave. Polyvinyl alcohol (PVA, Mw ≈ 67000) was purchased from Shanghai Aladdin Biochemical Technology Co. Ltd., China. Micrometer alumina powder (SAO-050E) was obtained from Shandong Sinocera Functional Material Co., Ltd., China. It had a mean particle size of 1 μm and a BET surface area of 2.49 m^2/g. Nanometer alumina powder (TM-DAR) was purchased from Taimei Chemicals Co. Ltd., Japan. It had a mean particle size of 0.1 μm and a BET surface area of 13.1 m^2/g. Alumina sol (Snowchemical

S&T Co., LTD, China) with a solid content of 20 wt% and a particle size of 10–20 nm was used. The mullite precursor was provided by the Institute of Chemistry, Chinese Academy of Sciences. It can be converted to a pure inorganic composition of 85 wt% Al_2O_3 and 15 wt% SiO_2 through thermal pyrolysis in air, and the conversion yield was 22 wt%.

2.2 Preparation of bulk ceramic samples

The aqueous ceramic slurry was prepared from organic glue, micrometer alumina powder, nanometer alumina powder (Fig. 1). The organic glue (PVA) content is 3 wt% with respect to the total amount of alumina components. The solid content of alumina components in the aqueous slurry was 33 wt%. The percentage of alumina sol in the alumina components was fixed to 25 wt%, and the ratios of micrometer alumina powder to nanometer alumina powder were tuned as follows: 10:1, 6:1, 4:1, 2:1, 1:2, and 1:10. The corresponding samples were referred to as M10, M6N1, M4N1, M2N1, M1N2 and N10, respectively. The samples were mixed by ball milling, and rotational speed and milling time was 600 r/min and 2 h, respectively. Afterwards, the aqueous slurry was dried, grounded and cold pressed to Φ 11×2 mm cylinder samples under 10 MPa. The cylinder samples decomposed at 500 ℃ in air for 2 h, and further sintered at a specified temperature for 2 h. The heating rate from room temperature to the decomposition and sintering temperature was set as 2 ℃/min.

2.3 Preparation of CMC samples

The Nextel 720™ fabric was cut into 3 cm · 3 cm pieces, on which the above aqueous slurries were spread with a brush, followed by drying the pieces in an air-circulating oven at 40 ℃. A hand lay-up process was employed to fabricate CMC samples. First, dried prepregs were wetted with aqueous slurry, nine pieces of whom were piled up in a metal mold and hot pressed at 100 ℃. After heat treatment for 1 h, samples were successively removed from the mold, post cured in a 200 ℃ of oven for 1 h, decomposed at 500 ℃ for 2 h, and pre-sintered at 900 ℃ for 2 h, to obtain a pristine CMC sample with the thickness around 2.1 mm and the fiber volume percentage about 45–48 %.

2.4 Impregnation and sintering of preceramic polymer

The pristine CMC sample was immersed in a cylinder container that was filled with mullite precursor solution. Then, the cylinder container was put in an autoclave, followed by maintaining the pressure and temperature as 2 MPa and 180 ℃ respectively for 2 h, to ensure the complete infiltration and curing of the mullite precursor inside the ceramic plate. After cooling down to room temperature, the sample was successively taken out, dried at 150 ℃, decomposed at 500 ℃, and pre-sintered at 900 ℃. The holding time for each process was 2 h. The whole procedure including infiltration, curing, decomposition, and pre-sintering was repeated several times (Fig. 1). In the last cycle, CMC sample was given a final treatment at 1150 ℃ for 2 h.

2.5 Characterization

The density of bulk ceramic samples and CMC samples was calculated according to the weight and volume of samples. The open porosity was measured on a Mettler-Toledo density kit according to the

Archimedes' principle. Three pieces of samples were used in each group to test the average bulk density, open porosity and linear shrinkage. The microstructure of samples was observed by scanning electron microscopy (SEM, JSM-7900F, JEOL, Japan). Mechanical properties of CMC samples were measured on a universal testing machine (AGS-X 1KN, Shimadzu, Japan) using an in-plane three-point bending mode with a span of 26 mm and a loading rate of 0.5 mm/min. Test specimens were cut into rectangle pieces (30 mm · 4 mm · 2.1 mm) by a diamond wire cutting machine. At least 5 samples per group were tested.

3. Result And Discussion

3.1 Microstructure and sintering behavior of bulk ceramic samples

Bulk ceramic samples with 3 wt% of organic glue (PVA), 25 wt% of alumina sol, and various ratios of micrometer alumina powders to nanometer alumina powders were prepared to investigate microstructure evolution and screen the suitable matrix composition. Bulk density, open porosity, and linear shrinkage of these samples sintered at different temperature are exhibited in Fig. 2. It can be seen that N10 bulk samples have the smallest bulk density before heat treatment as well as the highest open porosity when sintered at 800 ℃. In the same condition, M1N2 and M10 bulk samples have similar bulk density and open porosity, whereas M2N1, M4N1, and M6N1 bulk samples have the highest bulk density and the lowest open porosity. These results imply that the alumina components in M2N1, M4N1, and M6N1 bulk samples stacked more closely. The linear shrinkage of all these samples below 800 ℃ is low, revealing that these samples were not effectively sintered below 800 ℃. In the temperature range between 800 ℃～1000 ℃, the linear shrinkage of N10 gradually increases, suggesting that N10 samples can be slightly sintered during this temperature range. Above 1000 ℃, the linear shrinkage of N10 bulk samples demonstrates a sharp increase, revealing that nanometer alumina powders were effectively sintered. Correspondingly, its open porosity decreases dramatically, and bulk density increases rapidly. With the increase of the content of micrometer alumina powders, the change of bulk density, open porosity, and linear shrinkage gets slower than those of N10 samples, revealing that micrometer alumina powders have lower sintering activity and higher dimensional stability. The observation (Fig. S1-Fig. S5 in ESM) on microstructure evolution of bulk ceramic samples after sintering at various temperatures also supports this opinion. With the increasing temperature, nanometer alumina powders evidently grow and merge into large particles, whereas micrometer alumina powders remain their original shape up to 1500 ℃.

In sum, nanometer alumina powders have high sintering activity and poor dimensional stability. On the contrary, micrometer alumina powders possess excellent dimensional stability but lower sintering activity. The combination of nanometer and micrometer powders can offer the matrix with balanced sintering activity and dimensional stability. Among these compositions, M4N1 bulk samples demonstrate uniform distribution of nanometer and micrometer powders (Fig. 3), and possess relatively lower linear shrinkage and higher bulk density after thermal treatment at 1200 ℃ for 2h, suggesting that M4N1 may be used as a suitable matrix for CMC.

3.2 Microstructure and mechanical properties of CMC

Prepregs, prepared from aqueous slurry and Nextel 720™ fabric, were piled up by handcraft and hot pressed to form green body of CMC. After post curing, thermal decomposition, and pressureless sintering, CMC samples were obtained. Organic glue in aqueous slurry had twofold function, one was to stabilize inorganic particles and confer the hand lay-up processing ability, the other was to bind inorganic particles and ceramic fibers together below 200 ℃; From 200 ℃ on, the organic glue gradually decomposed and lost binding effect. Alumina sol continued to serve as an inorganic glue through chemical reaction of hydrogen bonds to avoid interlayer debonding under shrinkage stress; From 1000 ℃ on, alumina sol will be gradually consumed by alumina powders (Fig. S1-Fig. S5 in ESM). Nanometer alumina powders, attributed to their high sintering activity, will instead function as a bridge to hold inorganic particles together and offer CMC with mechanical strength; Micrometer alumina powders formed non-shrinking network and contributed to the high-temperature stability of CMC, because of their low sintering activity.

To enhance the mechanical performance of CMC, the preceramic polymer of mullite was introduced through twice impregnation process. Figure 4 shows that these CMC samples, except for N10 CMC samples, have similar flexural stress-strain curves. Among them, M4N1 CMC samples exhibit the largest maximum flexural stress value, although the difference with other samples is not so obvious. The flexural stress of these samples displays a step-wise drop phenomenon after reaching the maximum value, revealing that a series of events such as debonding between fibers and matrix, crack deflection, pulling out of fibers may occur to toughen the CMC. Pores in the matrix and between fibers and matrix may also have positive effects on toughening the CMC materials, since open porosity is still as high as 28% (Fig. 5) after two cycles of impregnation process.

3.3 Effects of preceramic polymer

To investigate the influence of preceramic polymer on mechanical performance of CMC, 0–5 times of impregnation process were conducted. The flexural stress-strain curves (Fig. 6a) of CMC samples exhibit the quasi-plastic behavior without impregnation of preceramic polymer. The maximum flexural stress of the CMC with one cycle of impregnation process increases from 101 MPa to 156 MPa. When two cycles of impregnation process are done, a peak value of 255 MPa is reached. However, as shown in Fig. 6b, extra cycles would cause the slight decrease of maximum flexural stress and shorter plateau beyond the maximum value. The possible reason is that toughening effects from debonding, crack deflection, and pulling out of fibers were diminished, due to the strong binding force between matrix and fibers and decreasing porosity (Fig. 7), brought by the overdosed preceramic polymer. It can be seen that from Fig. 8, the length of pulling out fibers becomes shorter as the impregnation cycles increase, suggesting that brittle fracture was prone to occur, and the toughening effects of ceramic fibers were weakened above two cycles of impregnation process.

3.4 Evaluation of high-temperature stability

The stress-strain curves of CMC samples after thermal exposure in air display in Fig. 9. As holding time at 1100 ℃ increases, the maximum flexural stress of CMC samples gets lower, but it still exhibits quasi-plastic deformation, suggesting the existence of multiple toughening mechanism. After the treatment at 1100 ℃ for 24 h, the strength retention rate is still around 85 %, proving the good high-temperature stability. As for the reason for slight decrease of mechanical performance, it might be related with the growth of grains in ceramic fibers, matrix, and ceramic coating from preceramic polymer (Fig. S6 in ESM). The grain growth will lead to the shrinkage of matrix and interlayer stress, and finally deteriorate the mechanical performance of CMC.

Conclusions

In this work, an aqueous ceramic slurry was designed for the preparation of oxide-oxide CMC, which included organic glue (PVA), alumina sol, micrometer alumina powder, nanometer alumina powder. The roles of different components were systematically elucidated. The optimized combination (PVA 3 wt%, alumina sol 25 wt%, M4N1) endowed CMC with good processing ability, high sintering activity and excellent thermal resistance simultaneously. In addition, the preceramic polymer of mullite was introduced by multiple impregnation process to enhance the mechanical performance of CMC. It was clarified that the impregnation cycles played an important role on mechanical performance of CMC. Two cycles can obviously promote the maximum flexural stress of CMC from 100 MPa to 255 MPa. However, overdosed mullite will cause inferior mechanical performance due to the change of fracture mechanism from ductile fracture to brittle fracture. In return, it implies us that mechanical performance might be further improved through proper interface engineering in future work. This study not only provides a facile and efficient method to prepare oxide-oxide CMC, but also can deepen our understanding about the microstructure evolution and functions of different alumina sources as the matrix of CMC.

Declarations

Acknowledgements

The authors gratefully acknowledge the financial support from National Natural Science Foundation of China (No. 21805092 and 52003272), Beijing Natural Science Foundation of China (No. 2204101), the Recruitment Program of Guangdong (No. 2016ZT06C322), and Guangdong Provincial Key Laboratory of Functional and Intelligent Hybrid Materials and Devices (No. 2019B121203003)

References

1. Almeida RSM, Bergmüller EL, Eggert BGF et al (2016) Thermal Exposure Effects on the Strength and Microstructure of a Novel Mullite Fiber. J Am Ceram Soc 99(5):1709–1716
2. Lanser RL, Ruggles-Wrenn MB (2016) Tension-Compression Fatigue of a Nextel™720/alumina Composite at 1200°C in Air and in Steam. Appl Compos Mater 23(4):707–717

3. Corman GS, Luthra KL (2018) Development History of GE's Prepreg Melt Infiltrated Ceramic Matrix Composite Material and Applications. In: Beaumont PWR, Zweben CH (eds) Comprehensive Composite Materials II. Elsevier, Oxford, pp 325–338
4. Hay RS, Keller KA, Zawada LP et al Degradation of Nextel™ 610-based oxide-oxide ceramic composites by aluminum oxychloride decomposition products. 2018, 101(9): 4203–4223
5. Jiang R, Sun X, Liu HT et al (2021) Microstructure and mechanical properties improvement of the Nextel™ 610 fiber reinforced alumina composite. J Eur Ceram Soc 41(10):5394–5399
6. Ruggles-Wrenn MB, Minor SN, Przybyla CP, *et al.* Creep of a Nextel™720/alumina ceramic composite containing an array of small holes at 1200°C in air and in steam. *1546-542X* 2019, **16**(1): 3–13
7. Jiang R, Yang L, Liu HT et al (2018) High-temperature mechanical properties of Nextel™ 610 fiber reinforced silica matrix composites. Ceram Int 44(13):15356–15361
8. Poges S, Monteleone C, Petroski K et al (2017) Preparation and characterization of an oxide-oxide continuous fiber reinforced ceramic matrix composite with a zinc oxide interphase. Ceram Int 43(18):17121–17127
9. Ben Ramdane C, Julian-Jankowiak A, Valle R et al (2017) Microstructure and mechanical behaviour of a Nextel™610/alumina weak matrix composite subjected to tensile and compressive loadings. J Eur Ceram Soc 37(8):2919–2932
10. Ruggles-Wrenn MB, Ozer M (2010) Creep behavior of Nextel™720/alumina–mullite ceramic composite with ± 45° fiber orientation at 1200°C. Mater Sci Eng A 527(20):5326–5334
11. Antti ML, Lara-Curzio E, Warren R (2004) Thermal degradation of an oxide fibre (Nextel 720)/aluminosilicate composite. J Eur Ceram Soc 24(3):565–578
12. Kaya C, Butler EG, Selcuk A et al (2002) Mullite (Nextel™ 720) fibre-reinforced mullite matrix composites exhibiting favourable thermomechanical properties. J Eur Ceram Soc 22(13):2333–2342
13. Ruggles-Wrenn MB, Whiting BA (2011) Cyclic creep and recovery behavior of Nextel™720/alumina ceramic composite at 1200°C. Mater Sci Eng A 528(3):1848–1856
14. Hay RS, Armani CJ, Ruggles-Wrenn MB et al (2014) Creep mechanisms and microstructure evolution of Nextel™ 610 fiber in air and steam. J Eur Ceram Soc 34(10):2413–2426
15. Armani CJ, Ruggles-Wrenn MB, Hay RS et al (2013) Creep and microstructure of Nextel™ 720 fiber at elevated temperature in air and in steam. Acta Mater 61(16):6114–6124
16. Wilson DM (1997) Statistical tensile strength of Nextel™ 610 and Nextel™ 720 fibres. J Mater Sci 32(10):2535–2542
17. Levi CG, Yang JY, Dalgleish BJ et al (1998) Processing and Performance of an All-Oxide Ceramic Composite. J Am Ceram Soc 81(8):2077–2086
18. Wang Y, Liu HT, Cheng H, *et al.* Fabrication and properties of 3D oxide fiber-reinforced Al_2O_3–SiO_2–SiOC composites by a hybrid technique based on sol–gel and PIP process. *Ceram Int* 2015, **41**(1, Part B): 1065–1071

19. Wang Y, Liu HT, Cheng HF et al (2014) Effective fugitive carbon coatings for the strength improvement of 3D Nextel™ 440/aluminosilicate composites. Mater Lett 126:236–239
20. Johnson SM, Blum Y, Kanazawa C et al (1998) Low-cost matrix development for an Oxide-Oxide composite. Me Mater Int 4(6):1119–1125
21. Guglielmi PO, García DE, Hablitzel MP et al (2016) Processing of All-Oxide Ceramic Matrix Composites with RBAO Matrices. J Ceram Sci Technol 7(1):87–96
22. Goushegir SM, Guglielmi PO, da Silva JGP et al (2012) Fiber-matrix compatibility in an All-Oxide ceramic composite with RBAO Matrix. J Am Ceram Soc 95(1):159–164
23. Fair GE, Hay RS, Boakye EE (2007) Precipitation coating of monazite on woven ceramic fibers: I. feasibility. J Am Ceram Soc 90(2):448–455
24. Fair GE, Hay RS, Boakye EE (2008) Precipitation coating of monazite on woven ceramic fibers: II. effect of processing conditions on coating morphology and strength retention of Nextel™ 610 and 720 fibers. J Am Ceram Soc 91(5):1508–1516
25. Fair GE, Hay RS, Boakye EE et al (2010) Precipitation coating of monazite on woven ceramic fibers: III—coating without strength degradation using a phytic acid precursor. J Am Ceram Soc 93(2):420–428
26. Richter H, Peters PWM (2016) Tensile strength distribution of all-oxide ceramic matrix mini-composites with porous alumina matrix phase. J Eur Ceram Soc 36(13):3185–3191

Figures

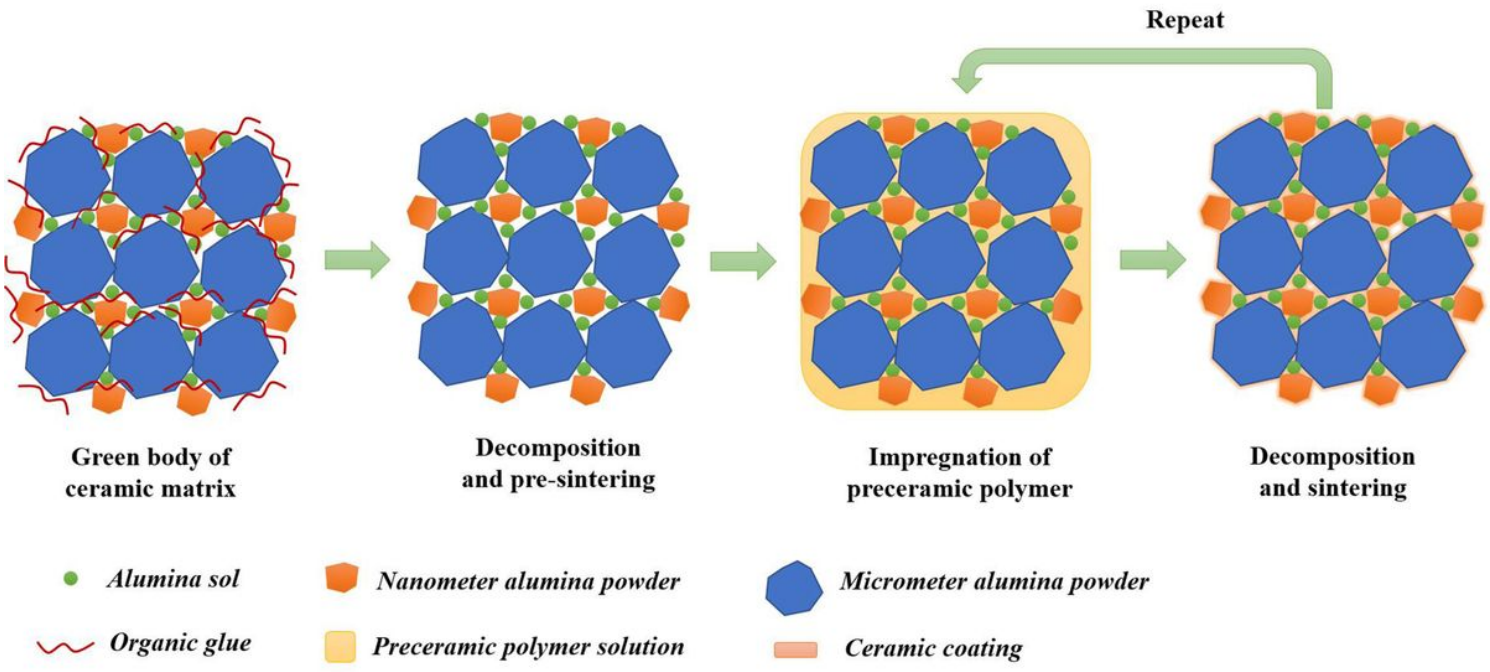

Figure 1

Design concept and route of the matrix in CMC.

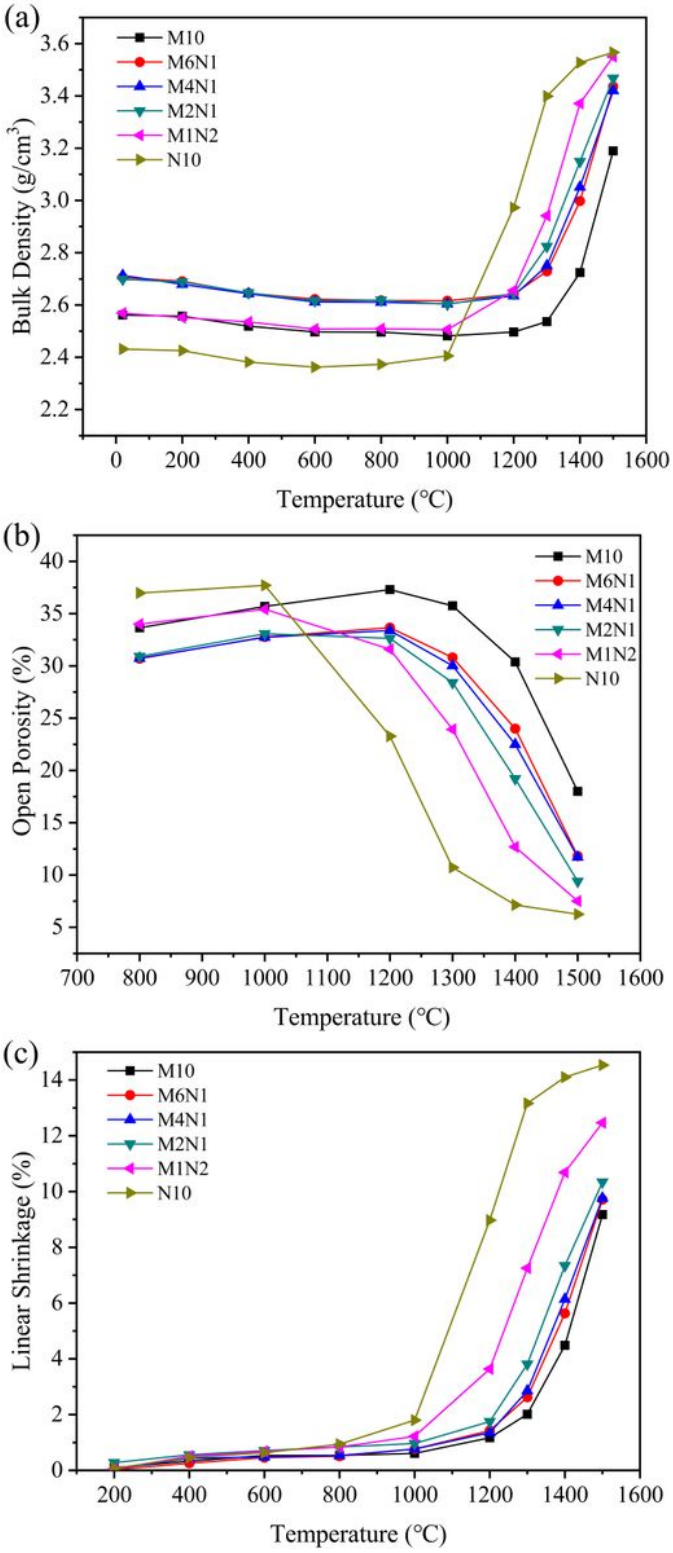

Figure 2

Effects of sintering temperature on the properties of bulk ceramic samples: (a) Bulk density, (b) Open porosity, (c) Linear shrinkage.

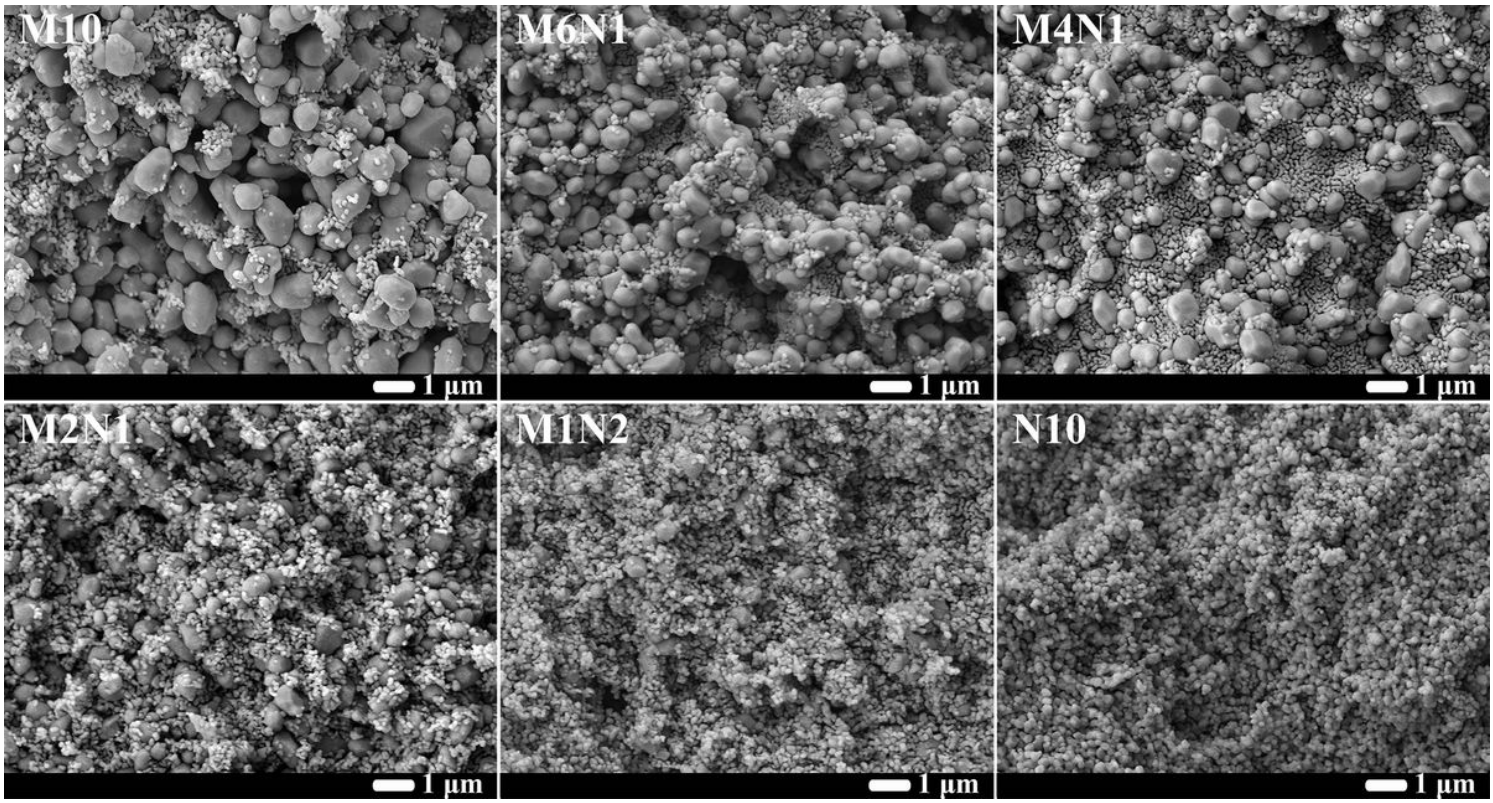

Figure 3

Cross-sectional SEM images of bulk ceramic samples sintered at 1200℃ for 2h.

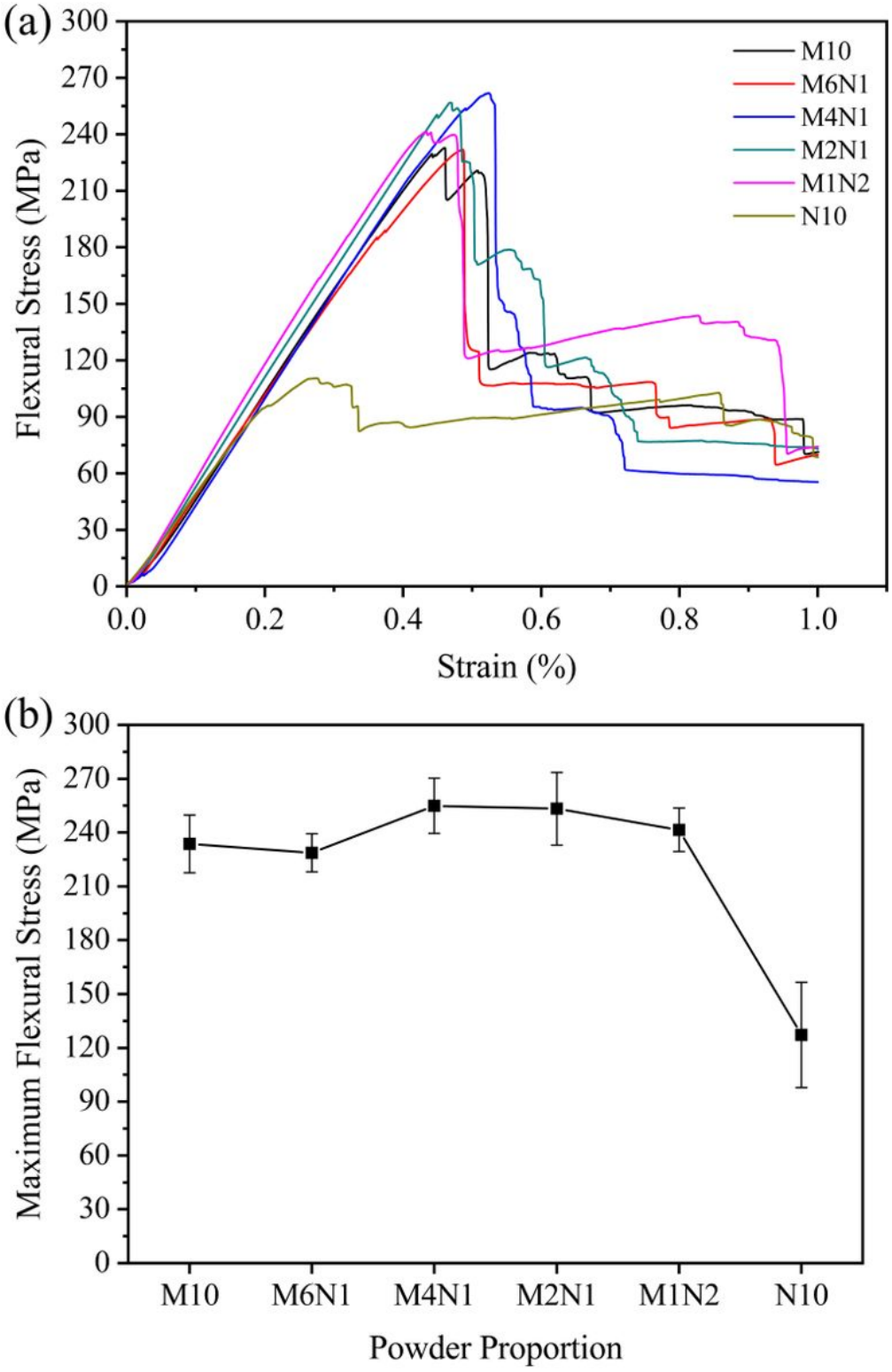

Figure 4

(a) Flexural stress-strain curves and (b) Maximum flexural stress of CMC with different compositions after two cycles of impregnation of preceramic polymer.

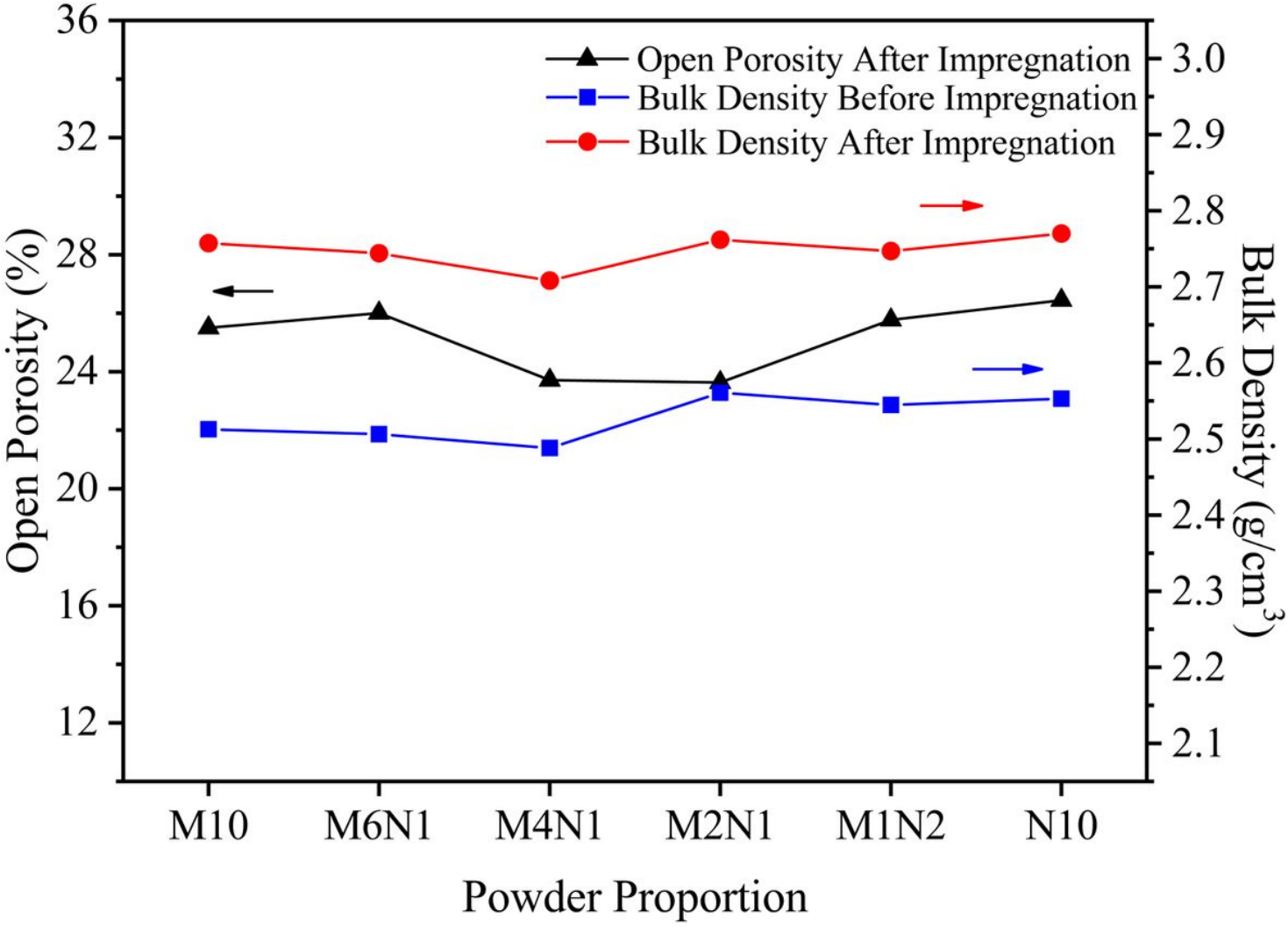

Figure 5

Open porosity and bulk density of CMC with different compositions.

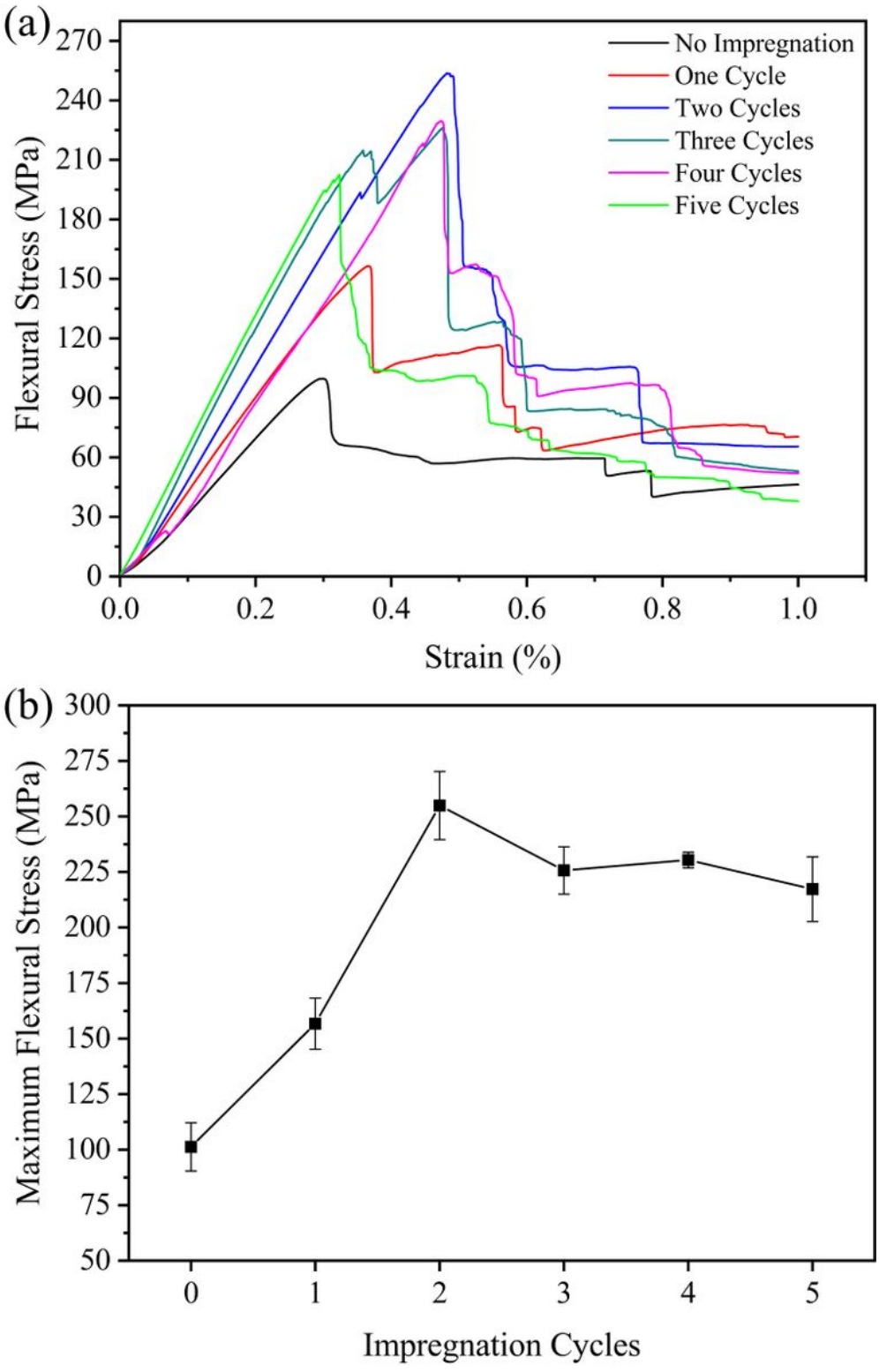

Figure 6

(a) Flexural stress-strain curves and (b) Maximum flexural stress of M4N1 CMC samples with different impregnation cycles of preceramic polymer.

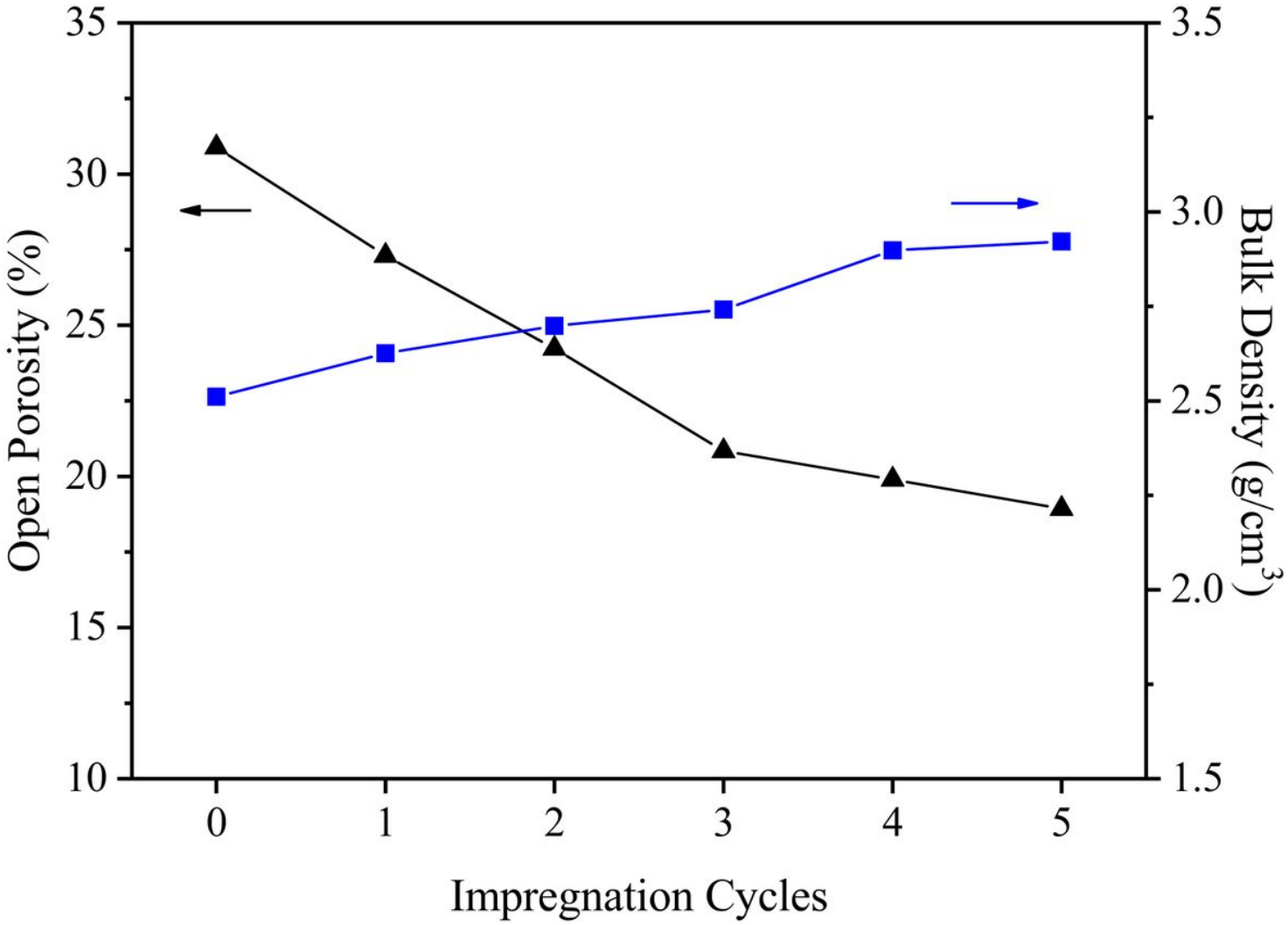

Figure 7

Open porosity and bulk density of M4N1 CMC samples with different impregnation cycles of preceramic polymer.

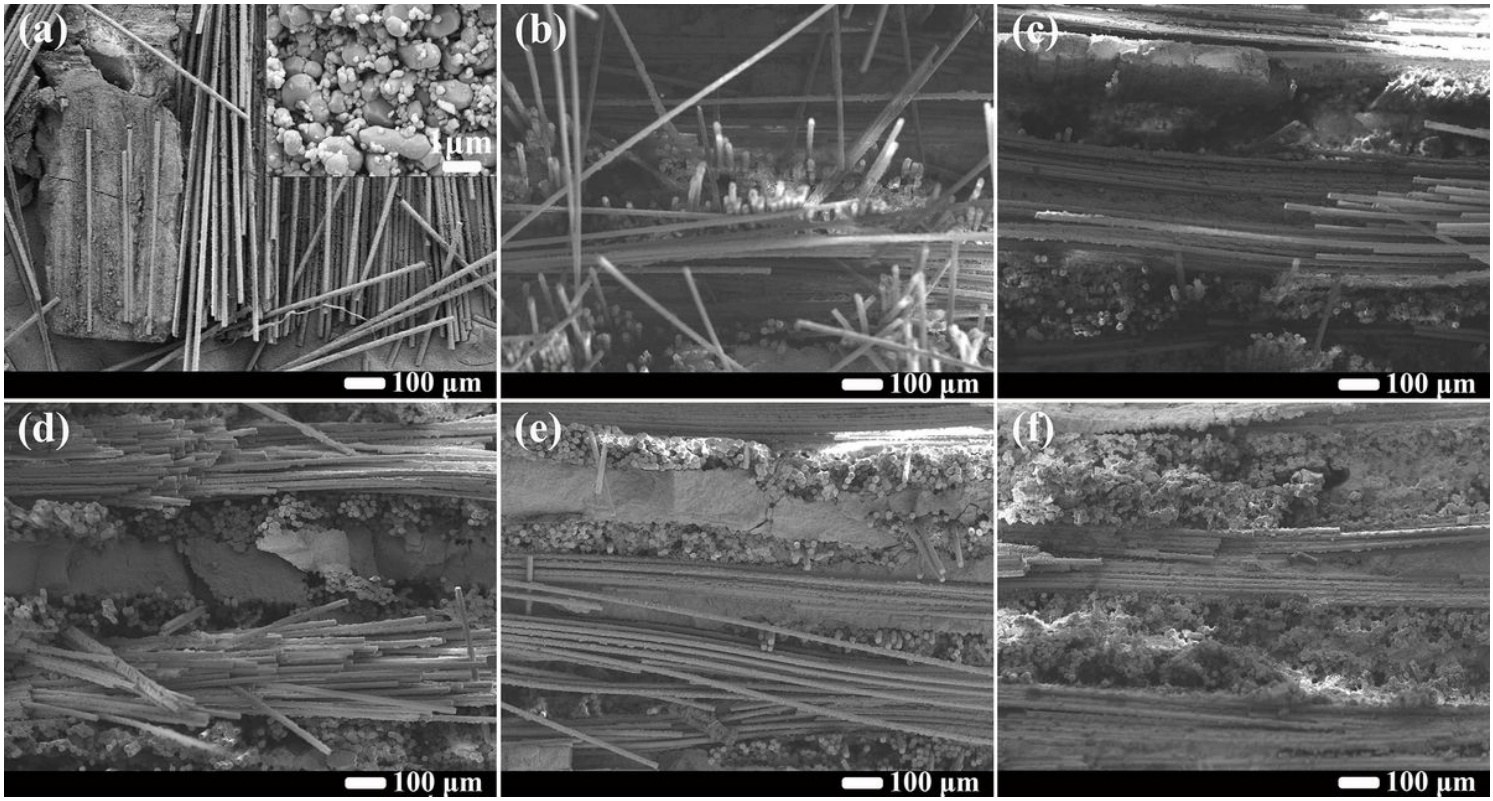

Figure 8

Cross-sectional SEM images of M4N1 CMC samples with different impregnation cycles of preceramic polymer: (a) None impregnation, (b) One impregnation, (c) Two impregnation cycles, (d) Three impregnation cycles, (e) Four impregnation cycles, (f) Five impregnation cycles.

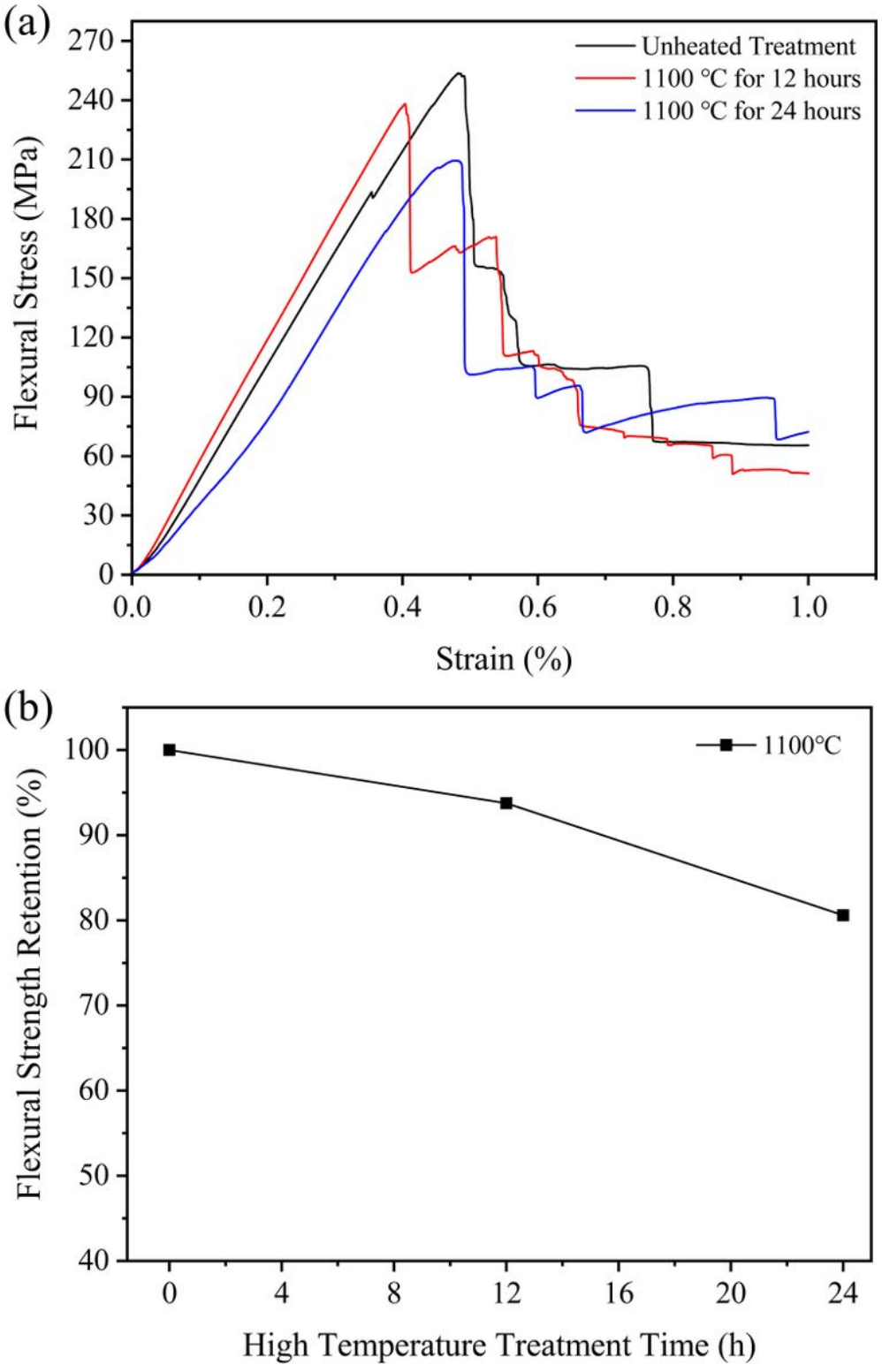

Figure 9

Effect of thermal exposure on the ambient mechanical properties of M4N1 CMC after two impregnation cycles of preceramic polymer: (a) Flexural stress-strain curves and (b) Flexural strength retention.

Supplementary Files

This is a list of supplementary files associated with this preprint. Click to download.

- supportinformation.docx